Research Article | Vol. 31, No. 12 / 5 Jun 2023 / Optics Express 20398
Optics EXPRESS

Optomechanically induced optical trapping system based on photonic crystal cavities

MANUEL MONTERROSAS-ROMERO,[1,2] SEYED K. ALAVI,[1,2] ESTER M. KOISTINEN,[1] AND SUNGKUN HONG[1,2,*]

[1]Institute for Functional Matter and Quantum Technologies, Universität Stuttgart, 70569 Stuttgart, Germany
[2]Center for Integrated Quantum Science and Technology (IQST), University of Stuttgart, 70569 Stuttgart, Germany
[*]sungkun.hong@fmq.uni-stuttgart.de

Abstract: Optical trapping has proven to be a valuable experimental technique for precisely controlling small dielectric objects. However, due to their very nature, conventional optical traps are diffraction limited and require high intensities to confine the dielectric objects. In this work, we propose a novel optical trap based on dielectric photonic crystal nanobeam cavities, which overcomes the limitations of conventional optical traps by significant factors. This is achieved by exploiting an optomechanically induced backaction mechanism between a dielectric nanoparticle and the cavities. We perform numerical simulations to show that our trap can fully levitate a submicron-scale dielectric particle with a trap width as narrow as 56 nm. It allows for achieving a high trap stiffness, therefore, a high Q-frequency product for the particle's motion while reducing the optical absorption by a factor of 43 compared to the cases for conventional optical tweezers. Moreover, we show that multiple laser tones can be used further to create a complex, dynamic potential landscape with feature sizes well below the diffraction limit. The presented optical trapping system offers new opportunities for precision sensing and fundamental quantum experiments based on levitated particles.

1. Introduction

Optical trapping is a versatile tool in modern science. Since its birth [1], optical trapping has been used in various groundbreaking experiments across disciplines, ranging from trapping and cooling of atoms [2] to the manipulation of individual living cells [3]. Recently, optical trapping has also found its utility in quantum optomechanics [4,5]. In high vacuum, a dielectric nanoparticle trapped in an optical tweezer becomes an excellent mechanical oscillator with an ultrahigh quality factor Q. It has allowed the observation and control of the particle's motion at the quantum limit [6–8], paving the way for new sensing technologies [9–11] and probing quantum physics in new mass and length scales [12–14].

However, there also exist outstanding challenges to further advancing tweezer-based quantum optomechanics. Realizing a high Q-frequency product of the mechanical oscillator [15,16] is an essential prerequisite for performing precision and quantum-coherent experiments [17]. With standard optical tweezers, it is achieved by increasing the tweezer beam's intensity, thus, the stiffness of the trap in which the particle oscillates. However, the intense laser field often also causes excessive absorption heating of the particle, in particular in high vacuum, and can result in the instability or even loss of the particle [18]. Even if the particle survives the heating-induced instability, the increased blackbody radiation could severely limit the system's coherence, thus precluding quantum experiments that require exceptionally long coherence times [12–14]. The trap stiffness can alternatively be enhanced by reducing the width of the trap. However, this

#489688 https://doi.org/10.1364/OE.489688
Journal © 2023 Received 16 Mar 2023; revised 7 May 2023; accepted 18 May 2023; published 1 Jun 2023

Optics EXPRESS

possibility is also limited for a conventional optical trap, as the length scale over which the trap can vary is bound by the diffraction limit.

In the meantime, researchers have studied a different trapping mechanism that could potentially circumvent the abovementioned limitations [19–21]. It utilizes optical nanocavities as a means to provide localized optical trapping fields. When external lasers pump the cavities, the optical gradient forces generated by the cavity fields can attract and trap particles nearby. The key difference to conventional optical tweezers is that the particles also strongly affect the trapping fields by shifting the cavities' resonance frequencies. This optomechanically-induced dynamic effect, also termed self-induced backaction (SIBA), results in an optical trap that is qualitatively different from standard optical tweezers. The SIBA effect has been first observed experimentally with a plasmonic nanocavity [20] and later with a dielectric photonic crystal cavity [21]. Recently, SIBA-based optical trapping was theoretically investigated in the context of optomechanics [22]. In this study, Neumeier et al. [22] have considered a simple Fabry-Perot cavity model and shown that the SIBA effect can produce optical traps with nontrivial shapes and sub-diffraction features if the cavity supports strong optomechanical interaction and sharp optical resonance. The next step is to devise a concrete cavity system that satisfies the required conditons for realizing low-intensity and high-stiffness optical levitation.

In this article, we present a nanophotonic cavity system that can practically realize a high-stiffness SIBA trap for a dielectric nanoparticle. Our trap is based on two photonic crystal nanobeam cavities (PCNC) that can be conveniently made using conventional nanofabrication technologies. The PCNC's high Q factor and the strong optomechanical response can result in enhanced SIBA effects that substantially modify the optical gradient force by the cavity field. We show that two PCNCs arranged in parallel, when pumped with appropriate laser fields, can form an optical trap with a width close to 50 nm. It dramatically reduces the optical field intensity required for a desired trap stiffness by a factor larger than 40. In contrast to previously demonstrated SIBA traps [20,21], the particle in our trap is fully levitated without any physical contact with the PCNCs. The particle can thus attain excellent mechanical coherence and stability in high vacuum. We also demonstrate the capability of our PCNC-based trap to create a more complex potential landscape, which is achieved by pumping the PCNCs with multiple laser fields.

2. Concept of the PCNC-based SIBA trap

The central component of our trap is a photonic crystal nanobeam cavity (PCNC) (Fig. 1(a)). PCNCs have already been exploited to realize an efficient near-field trap [23,24] as they provide strong optical gradient forces through the evanescent fields. The PCNCs can also exhibit strong SIBA effects because their high-Q resonant optical modes can dynamically respond to a slight change in the local dielectric environment by an external dielectric object. Specifically, a nearby dielectric particle increases the effective optical path length near the cavity, thus decreasing the resonance frequencies of the cavity. This resonance frequency shift becomes more prominent as the particle approaches closer to the PCNC, resulting in a position-dependent frequency shift of the PCNC. It has been previously observed that the displacement of a nearby glass nanoparticle by 100 nm can result in the shift of the PCNC's frequency shift by 1 GHz [25]. Considering typical linewidths of the PCNC's resonances are on the order of GHz [26], the shift is enough to change the intensity of the cavity field significantly.

A prerequisite for quantum optomechanics experiments is levitating the particle without direct contact with the PCNCs. Otherwise, surface friction would immediately destroy any quantum coherence of the particle. However, with a single PCNC, surface contact would be unavoidable, as an optical gradient force from a PCNC is always attractive. We solve this problem by additionally employing another PCNC on the other side of the particle (Fig. 1(b)). This scheme first allows for balancing the attractive force from one PCNC with the same pull from the other. Next, suppose the particle is slightly displaced from the force equilibrium position. In that case, the SIBA

Optics EXPRESS

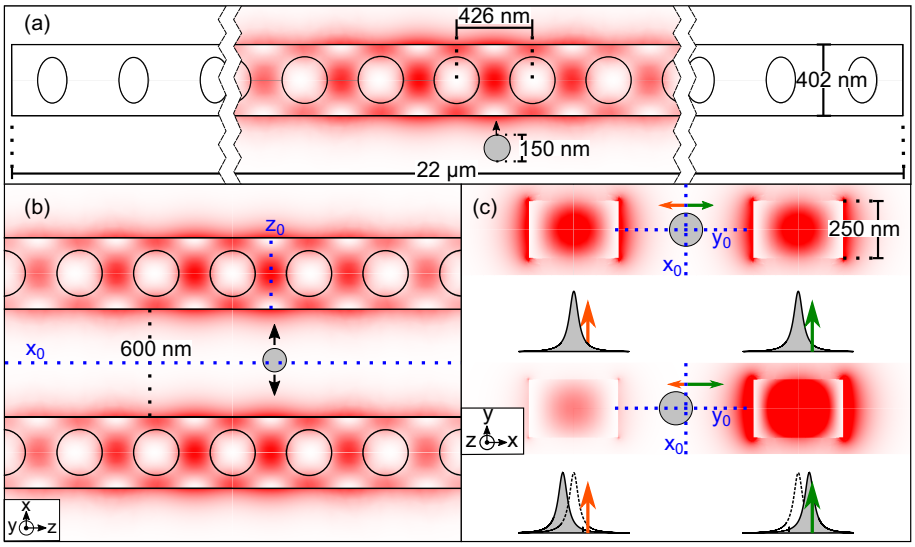

Fig. 1. Working principle of the PCNC-based SIBA trap **a.** Simulated electric field intensity of a silicon photonic crystal nanobeam cavity (PCNC) used in our study. The PCNC is designed to be 22 μm in length and 402 nm in width. At each side of the PCNC, an array of holes is created to form a Bragg mirror. These hole arrays are extended to the center of the PCNC with the hole size and spacing properly tapered to form a localized cavity mode. When a 150 nm silica nanosphere (a light gray circle) is brought near a single PCNC, the particle is attracted to the PCNC due to the optical gradient force by the cavity's evanescent field. **b.** A layout of a PCNC-based self-induced backaction (SIBA) trap. Two PCNCs are placed in parallel with a distance of 600 nm. The inset in the bottom left corner shows the coordinate system used throughout the article. The x and z coordinates of its origin, (x_0, y_0, z_0), are also depicted; the plane of $x = x_0$ lies precisely in the middle between the two PCNCs, and the $z = z_0$ plane lies in between the cavity hole at the center and the neighboring hole, where the maximum of the cavity's evanescent field is located. The $y = y_0$ plane cuts through the middle of the PCNCs in the y direction (shown in (c)). **c.** Schematic illustration of restoring optical forces arising from SIBA effect. A 150 nm silica nanosphere is initially positioned at the origin (x_0, y_0, z_0). When the two PCNCs are pumped with equal laser power and detuning, the optical pulling forces on the particle are balanced when the particle is at the origin. When the particle is displaced to one of the PCNCs, e.g., on the left, the SIBA effect shifts the cavities' resonance frequencies such that the cavity field intensity on the left is substantially reduced while the field intensity on the right is increased, creating an imbalance in the magnitude of the two optical pulling forces. It results in a net force pushing the particle back toward the origin, keeping the particle in between the two PCNCs. We note that this picture holds until the cavity frequency of the PCNC on the right is brought into resonance with the laser pump frequency. If the displacement is increased further, the resonance frequency of the PCNC will shift past the laser frequency, resulting in the extinction of the cavity field as well (see Fig. 3 for more detail).

Optics EXPRESS

effects will induce resonance frequency shifts of the two PCNCs in opposite directions, creating a drastic imbalance of the cavity field strengths and respective optical pulling forces. When the detunings of the laser pumps are chosen appropriately, the sum of the two forces can result in a net restoring force that pushes the particle back to its original position (Fig. 1(c)). This mechanism makes it possible to stably keep the particle fully levitated from the two PCNCs.

3. Numerical analysis of the PCNC-based SIBA trap

To investigate the feasibility of the PCNC-based SIBA trap, we perform a series of numerical analyses with realistic PCNC designs and experimental parameters. As a device used to create the SIBA trap, we consider a silicon PCNC with a tapered hole array (Fig. 1(a)) [26]. Silicon PCNCs have been used extensively in various applications [23,27,28] and proven to exhibit quality factors up to 1.22×10^6 (or intrinsic cavity decay rate down to $\kappa_{in}/2\pi = 160$ MHz) at telecommunication wavelengths [29]. We use finite element method (FEM) simulations to design and optimize a free-standing silicon PCNC to have its resonance wavelength at 1550 nm. The simulated intrinsic cavity loss rate is found to be 40 MHz, which is hard to achieve from real devices due to imperfections and contaminations associated with fabrication processes. We instead use the previously demonstrated value of 160 MHz [29] as a realistically achievable cavity loss. Considering additional loss channels introduced by nearby PCNC and particle (see Supplement 1), the total cavity internal loss rate is assumed to be $\kappa_{in}/2\pi = 370$ MHz. In addition, we assume the coupling rate between the cavity and the input optical mode ($\kappa_{ex}/2\pi$) is 80 MHz, resulting in the total cavity loss rate $\kappa/2\pi = \kappa_{in}/2\pi + \kappa_{ex}/2\pi = 450$ MHz.

Next, we examine how the PCNC is influenced by a nearby dielectric nanoparticle, i.e., the shift of the PCNC's cavity frequency as a function of the particle's position. Here we consider a silica nanosphere with a diameter of 150 nm as the particle, which is widely used in quantum optomechanics experiments based on optical tweezers [7,8,30]. The cavity frequency shift $\Delta\omega_c(\vec{r}) \equiv \omega_c(\vec{r}) - \omega_0$, where $\omega_c(\vec{r})$ is the cavity frequency when the particle is at a position $\vec{r}$, and ω_0 is the unperturbed cavity frequency, can be obtained by conducting the FEM simulation of the PCNC with the particle placed at a given position $\vec{r}$. However, obtaining a full map of $\Delta\omega_c(\vec{r})$ requires repeating the simulations while sweeping the particle position as a parameter, which is computationally costly. Instead, we choose to use the following approximate expression derived from perturbation theory [5]:

$$\Delta\omega_c(\vec{r}) \approx -\frac{\omega_0}{2}\frac{(\varepsilon_p - 1)|\vec{E}(\vec{r})|^2 V_p}{\int_{PCNC}\varepsilon_m(\vec{r}')|\vec{E}(\vec{r}')|^2 dV' + \int_{air}|\vec{E}(\vec{r}')|^2 dV'} \tag{1}$$

where ε_p and ε_m are dielectric constants of the particle and the PCNC (i.e., silicon) respectively, V_p is the volume of the particle, and $\vec{E}(\vec{r})$ is the electric field of the cavity mode in the absence of the particle. The validity of Eq. (1) is confirmed by comparing the values obtained from it with the results from the brute-force simulation including the particle for several particle positions (see Supplement 1, Fig. S1). Equation (1) allows us to obtain a complete map of $\Delta\omega_c(\vec{r})$ from a single simulation of the cavity field distribution of the unperturbed PCNC, drastically reducing computational overhead. Figure 2(a) shows the two-dimensional plane cut of $\Delta f_c = \Delta\omega_c/2\pi$ across the cavity center. When the particle is brought within 300 nm from the surface of the PCNC, a frequency shift of around 1 GHz is anticipated. Moreover, an additional displacement of the particle's position by 40 nm is enough to shift the cavity's frequency more than the assumed linewidth of 450 MHz (Fig. 2(b)). Therefore, a strong SIBA effect is expected already at the distance of 300 nm.

As described earlier, our trap consists of two parallel PCNCs placed sufficiently close to each other. We assume the two PCNCs are nearly identical, having the same cavity loss rate and frequency shift response (i.e., $\Delta\omega_c(\vec{r})$) to the particle. However, we require the PCNCs

Optics EXPRESS

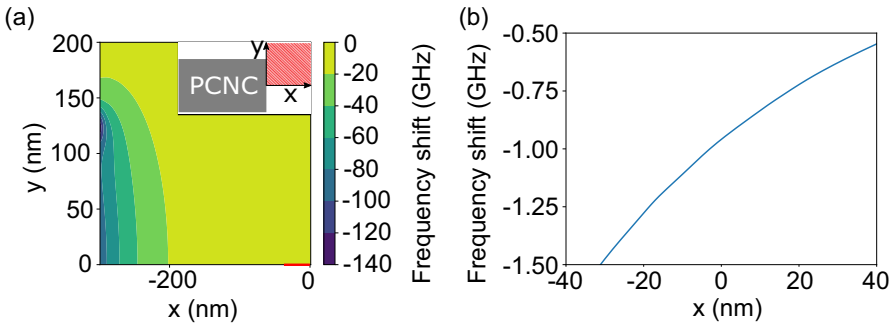

Fig. 2. Optomechanical coupling between the PCNC and the particle **a.** Shown is the map of the PCNC's resonance frequency shift caused by the nanoparticle on a plane at $z = z_0$. The inset indicates the relative location between the mapped area and the PCNC. **b.** The line cut of the frequency shift zoomed in around the origin. The location and the span of the line cut are depicted as a red line near the bottom-right corner in (a). The particle's displacement of 40 nm around $x = 0$ is enough to shift the cavity's frequency by around more than the assumed linewidth of 450 MHz.

to have different resonance frequencies such that the evanescent fields from the two cavities, when pumped with the same detuning from each resonance, do not result in interference. The surface-to-surface distance of the two PCNCs is assumed to be 600 nm as it is large enough to comfortably accommodate a 150 nm diameter particle and tolerate fabrication inaccuracies. At this distance, the influence of the two off-resonant PCNCs on each other is found to be negligible, only causing a slight increase in the loss rate (see Supplement 1). All the important parameters and conditions used in the analysis are summarized in Table 1.

Table 1. List of the parameters and their assumed values for the simulations

Parameter	Value	Note
Cavity resonance wavelenght, λ_c	~1550 nm	The resonances are assumed to be slightly different for each PCNC
Intrinsic cavity loss rate, $\kappa_{in}/2\pi$	370 MHz	
Total cavity loss rate, $\kappa/2\pi$	450 MHz	
Distance between the two PCNCs (surface-to-surface), d	600 nm	
Input power, P	30 μW	For each PCNC
Laser detuning, $\delta \equiv \omega_L - \omega_0$	$\kappa/\sqrt{3} + \Delta\omega_c(\vec{r}_0)$	$\Delta\omega_c(\vec{r}_0)$: the cavity resonance frequency shift by the particle at the origin $\vec{r}_0 = (x_0, y_0, z_0)$

The optical force by the PCNC on the particle can be directly computed from the shift of the PCNC's frequency [22] and is given by

$$\vec{F}(\vec{r}) = \hbar n(\vec{r})\vec{\nabla}\Delta\omega_c(\vec{r}) \tag{2a}$$

$$n(\vec{r}) = \frac{P}{\hbar\omega_L}\frac{\kappa_{ex}}{(\kappa/2)^2 + (\delta - \Delta\omega_c(\vec{r}))^2} \tag{2b}$$

where n is the intracavity photon number, which depends on the parameters given in Table 1 and the laser frequency ω_L. The above expression is obtained by ignoring the finite response time of the intracavity photon number to the particle-induced frequency shift [22] and is valid as long

Optics EXPRESS

as the bandwidth of the cavity ($\kappa/2\pi$ = 450 MHz) is much larger than the resulting oscillation frequency of the trapped particle, which will be confirmed later.

We now show how the particle can be levitated in our trap. To that end, we calculate the optical forces exerted on the particle (Fig. 3). Here we consider pumping each PCNC with the laser input power P = 30 μW and the laser detuning $\delta = \kappa/\sqrt{3} + \Delta\omega_c(\vec{r}_0)$, where $\Delta\omega_c(\vec{r}_0)$ is the cavity's resonance frequency shift when the particle is precisely in the middle between the two PCNCs (i.e., at position $\vec{r}_0 = (x_0, y_0, z_0)$ in our coordinate system). Of particular importance is the choice of the laser detuning, which consists of two terms. The term $\Delta\omega(\vec{r}_0)$ is the offset needed to compensate for the frequency shift when the particle is at the origin. The term $\kappa/\sqrt{3}$ then shifts the frequency from on-resonance to slightly off-resonance, allowing the SIBA effect to occur as described in Fig. 1. Figure 3(a) shows how the SIBA effect dramatically modifies the optical force. The small displacement of the particle at its original position (x = x_0 = 0 in Fig. 3(a)) can completely shift the cavity's resonance frequency out of resonance with the laser pump. This effect converts the monotonously increasing force profile into the one strongly peaked around the origin. Due to the nonlinearities of $n(\vec{r})$ and $\Delta\omega_c(\vec{r})$, the force profiles from the two PCNCs are asymmetric and shifted from each other; the sum of the two forces, therefore, gives rise to a net restoring force (Fig. 3(b)). Remarkable is that the change of the force occurs sharply within the length scale of less than 50 nm. This sharp, sub-diffraction feature of the force originates from the PCNC's narrow optical resonance that responds strongly to the particle's displacement. We also look at the forces along other spatial directions (Fig. 3(d), (f)) and confirm that they are also arranged to confine the particle in its origin. We note that the length scales over which the forces change are much larger than the one along the x direction because the SIBA effects are much less significant along those directions due to the modest frequency shift gradients (Fig. 3(c), (e)).

From Eq. (2), we find that the curl of the SIBA forces is zero, i.e., $\vec{\nabla} \times \vec{F}(\vec{r}) = 0$, implying that the work difference is path independent. This allows us to define the potential $U(\vec{r})$ by integrating the work from a fixed reference point in space $\vec{r}_{ref}$:

$$U(\vec{r}) = -\int_{\vec{r}_{ref}}^{\vec{r}} \vec{F} \cdot d\vec{r}' \tag{3}$$

We numerically compute the potential by choosing the point (x_{max}, y_0, z_0) as the reference point ($\vec{r}_{ref}$), where x_{max} = 300 nm corresponds to the point closest to the PCNC on the right. Figure 4 shows that our trap indeed forms a three-dimensional potential well. As already indicated in the force analysis, the full-width-at-half-maximum of the potential along the x direction is 56 nm, an order of magnitude smaller than the diffraction limit (Fig. 4(b)).

The depth of the potential appears to be close to 3 k_BT, where k_B is the Boltzmann constant and T = 300 K is the room temperature (Fig. 4(b)). This may not be sufficiently deep enough to fully ensure trap stability in high vacuum at room temperature. While the trap depth can be increased by increasing the input laser pump power, we also note that the active stabilization schemes by feedback cooling [31,32] are also readily available for our system; the frequency shifts of the PCNCs by the particle displacement also strongly change the intensities of the reflected pump laser fields, which can be measured to sensitively detect the position of the particle and fed back to modulate the laser fields to stabilize the particle's motion.

Spring constants of the trap and corresponding particle's oscillation frequencies can be extracted from the potential and are found to be (15.05 μN/m, 2.14 MHz), (1.15 μN/m, 595.2 kHz), and (0.76 μN/m, 484.12 kHz), respectively, along the x, y, and z directions. The highest frequency is sufficiently smaller than the cavity decay rate, confirming the validity of the approximation used in Eq. (2).

The strong restoring forces in our trap result from the cavity's sharp resonance, which converts optomechanically induced frequency shift to steep modulation of the cavity field. We observe that the restoring nature of our trap is still maintained when the linewidth is increased from

Optics EXPRESS

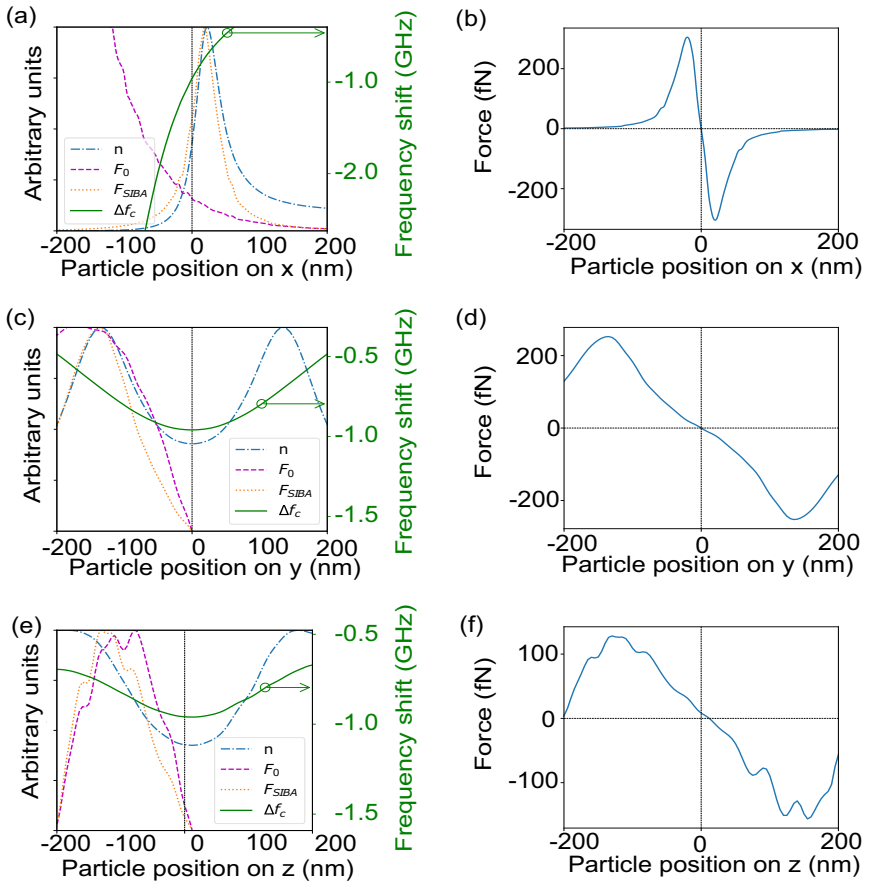

Fig. 3. a,c,e. Cavity frequency shift ($\Delta f_c = \Delta\omega_c/2\pi$; solid line), intracavity photon number (n; dash-dotted line), and resultant optical SIBA force (F_{SIBA}; dotted line) by a single PCNC (positioned at $x = -300$ nm) as a function of the particle's position along the x, y, and z directions. For comparison, optical gradient force by a single PCNC with a fixed intracavity photon number (F_0; dotted line) is also shown. The profiles are chosen to intersect with (x_0, y_0, z_0). The change of the frequency shift is significant along the x direction (a). Together with a narrow cavity resonance, it strongly modulates the intracavity photon number, thus resulting in the optical SIBA force sharply peaking at a length scale less than 50 nm. The frequency shift gradients along y and z directions, however, are moderate, inducing much weaker SIBA effects (c, e). The trends of the F_{SIBA} in these directions, therefore, do not show significant deviations from F_0. **b,d,f.** Net forces on the particle along x, y, and z directions, when the particle is placed in the PCNC-based SIBA trap. The centers of the line cuts coincide with (x_0, y_0, z_0). In all cases, forces on the negative coordinates are positive and vice versa, confirming the restoring action of the forces toward the origin. A strong SIBA effect along the x direction creates a steep force gradient within the narrow region at the trap center (b), while the forces in the other directions show much more gradual changes over larger length scales (d, f).

450 MHz to 900 MHz (Fig. 5). However, the stiffness and the potential depth are substantially decreased because the cavity with broader resonance does not respond as sharply to the frequency shift. It results in a shallower depth of the trapping potential. When the cavity linewidth exceeds

Optics EXPRESS

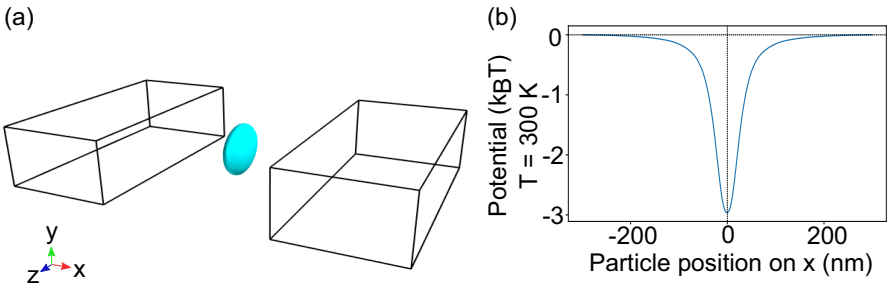

Fig. 4. a. Three-dimensional potential well formed by the PCNC-based SIBA trap. Shown is the equipotential surface with the potential value of $U = -1\,k_BT$ at room temperature (T = 300 K). The closed surface confirms that the trap can securely contain the particle in three dimensions. The larger extent of the potential along y and z directions is due to modest cavity frequency shift gradients along those directions, which result in weak SIBA effects. **b.** Potential profile along the x direction. The line cut was taken along $y = y_0$ and $z = z_0$. The width of the potential at half maximum is 56 nm, clearly featuring a length scale much smaller than the diffraction limit.

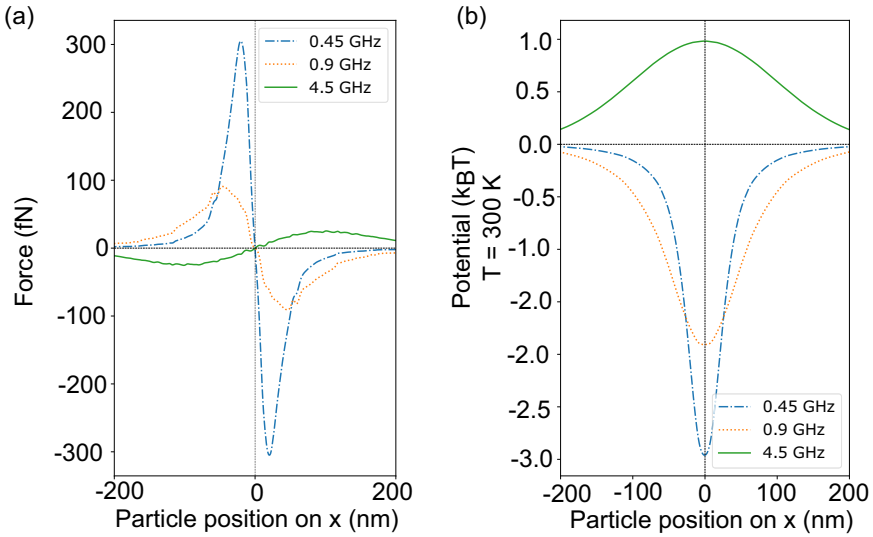

Fig. 5. a. Trapping forces on the particle along the x direction as a function of the particle's position for different decay rates $\kappa/2\pi$: 0.45 GHz, 0.9 GHz, and 4.5 GHz. The line cuts were taken along $y = y_0$ and $z = z_0$. The inset at the left-bottom corner shows the zoom-in of the $\kappa/2\pi = 4.5$ GHz case. As the decay rate increases, the magnitude of the restoring force decreases until it disappears. We found the turning point to be around 1.8 GHz. When the decay rate is further increased to 4.5 GHz, the polarity of the force is inverted, and the particle is pushed out from the center. **b.** The corresponding potentials along the x direction. As the decay rate is increased, the depth of the potential is reduced. When the decay rate is above 1.8 GHz, the potential is flipped such that the center of the potential becomes unstable.

a threshold (1.8 GHz in our design), our trap no longer forms a stable potential and loses the ability to confine a particle.

Figures 3 and 4 show that our system can form a high-stiffness optical trap (the spring constant of 15.05 μN/m and the corresponding particle's oscillation frequency of 2.14 MHz) only with 60 μW input power (30 μW input for each PCNC). With the same input power, a standard optical

Optics EXPRESS

tweezer with a numerical aperture (NA) of 0.95 would have resulted in a trap with a factor of 4600 less stiffness (a factor of 68 lower frequency) and a trap depth of only 0.06 k_BT at room temperature (see Supplement 1). This drastic reduction in the input power required for activating an effective trap is certainly one of the merits of our trapping scheme.

A more important parameter to consider is the optical field intensity that a particle would actually experience in a trap, as it is directly proportional to the absorption heating, which could induce the loss of the particle. We compare the field intensities the particle would see in the case of a standard optical tweezer and our PCNC-based trap when both traps are tuned to obtain the same trap stiffness (Fig. 6). Indeed, the field intensity at the center of the PCNC-based trap is a factor of 43 smaller than that of the standard optical tweezer. It primarily results from the difference in the trap width, which is inversely proportional to the square of the spring constant. We emphasize that the ability to generate a high stiffness trap with significantly reduced optical exposure is a critical feature of our trap, particularly for performing quantum optomechanics experiments; it allows the realization of a high Q-frequency product for the particle's motion while minimizing the possibility of optical damage to the particle.

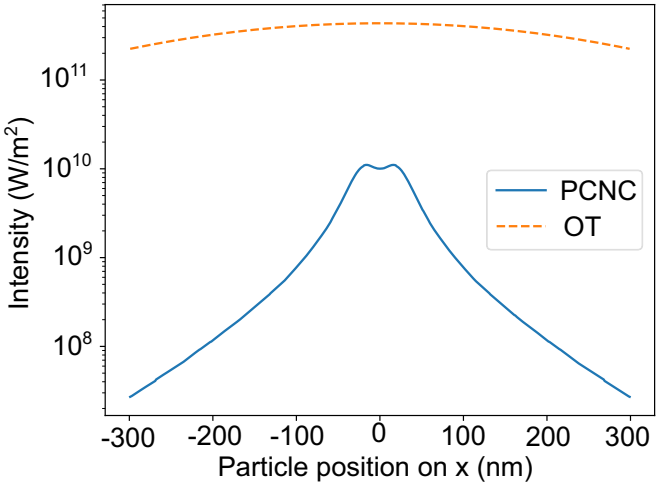

Fig. 6. Comparison of the optical field intensity that the particle (a silica nanosphere with 150 nm diameter) would see in a standard optical tweezer (OT) and the PCNC-based trap (PCNC). The intensity profiles are calculated assuming that both traps result in the same stiffness (i.e., the spring constant of 15.05 μN/m) along the x direction. The NA of the objective lens for the OT is assumed to be 0.95. The line cuts are taken along $y = y_0$ and $z = z_0$. At the center ($x = 0$) of the PCNC-based trap, the particle sees 43 times less intensity compared to the case for the OT.

The width of our trap (56 nm) is 18 times narrower than the diffraction-limited width of the standard optical tweezer (995 nm). If our trap were a standard opical trap made with a shorter wavelength laser, the width reduction would result in the reduction of the intensity at the trap center by a factor of $18^2 = 324$. The reason why this factor is not equal to the observed difference of 43 is that the PCNC-based trap is qualitatively different from standard optical traps. Indeed, Fig. 6 shows another distinctive feature of the PCNC-based trap; in clear contrast to the optical tweezer, the intensity maxima of the PCNC-based trap appear at both sides of the trap center, not at the trap center.

In operating the PCNC-based SIBA trap, the detuning δ of the input laser field plays a central role as it determines the regions where the cavity field is turned on. We use this principle to obtain further control in trap landscaping. First, we achieve a simple control in displacing the

Optics EXPRESS

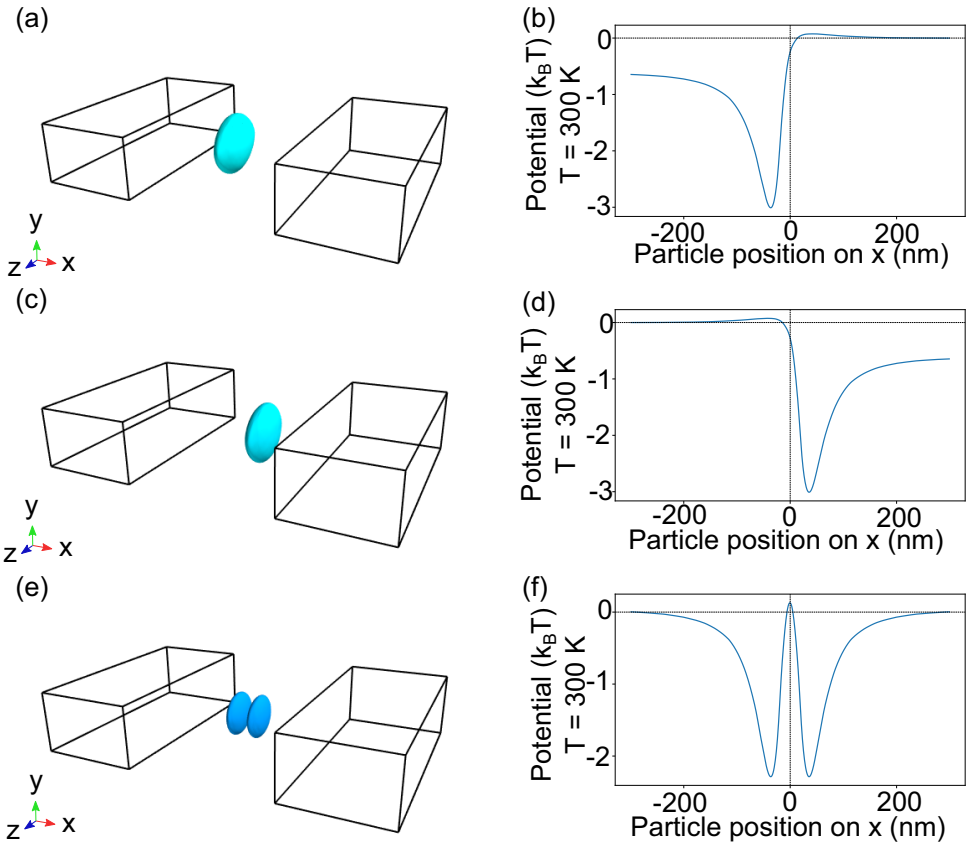

Fig. 7. **a.** The equipotential surface of the trap potential formed by choosing the laser detuning for the left PCNC $\delta_L = 2\kappa/\sqrt{3} + \Delta\omega_c(\vec{r}_0)$ and the detuning for the right PCNC $\delta_R = -\kappa/\sqrt{3} + \Delta\omega_c(\vec{r}_0)$. The value of the potential on the surfaces is fixed to $U = -1\,k_BT$. **b.** The line-cut of the corresponding potential along the x direction, taken at $y = y_0$ and $z = z_0$. The position of the trap center is moved to $x = -37$ nm. **c.** The equipotential surface ($U = -1\,k_BT$) of the trap potential with $\delta_L = -\kappa/\sqrt{3} + \Delta\omega_c(\vec{r}_0)$ and $\delta_R = 2\kappa/\sqrt{3} + \Delta\omega_c(\vec{r}_0)$. **d.** The line-cut of the corresponding potential along the x direction, taken at $y = y_0$ and $z = z_0$. The position of the trap center is $x = 36$ nm. For convenience, in Figs. c and d, the reference point r_{ref} has been changed to (x_{min}, y_0, z_0), where $x_{min} = -300$ nm. This makes it easier to compare side by side the asymmetric potentials. **e.** The equipotential surface ($U = -1\,k_BT$) of the double-well potential for a single nanoparticle formed by driving both PCNCs with two laser tones with the detunings $\delta_1 = -\kappa/\sqrt{3} + \Delta\omega_c(\vec{r}_0)$ and $\delta_2 = 2\kappa/\sqrt{3} + \Delta\omega_c(\vec{r}_0)$. **f.** The line-cut of the corresponding potential along the x direction, taken at $y = y_0$ and $z = z_0$.

trap by appropriately shifting the input laser detunings to both PCNCs (Fig. 7(a), (b), (c), (d)). More fascinating possibilities arise when both cavities are pumped with multiple laser tones with different amplitudes and detunings. One example is a double-well potential shown in Fig. 7(e). We realize it by pumping each PCNC with two laser tones which are used to create two displaced single-well traps. The width of each well and the separation between the wells are 53 nm and 72 nm, respectively, demonstrating the scheme's ability to create a potential landscape with a nanoscopic resolution. We anticipate this approach with multiple laser tones will offer a powerful method for creating more complicated potential landscapes beyond the diffraction limit,

Optics EXPRESS

which can be used, for instance, to study various outstanding problems involving single-particle dynamics [33] with enhanced resolutions.

4. Conclusion

In summary, we have shown that the optical trapping system formed by two parallel silicon PCNCs can levitate a silica nanoparticle with a diameter of 150 nm in a gap between the two PCNCs. Strong optomechanical interactions between the PCNCs and the particle dramatically modify optical forces from the cavities, resulting in extremely narrow trapping potential with a width of only 56 nm. The significantly reduced potential width allows for achieving the oscillation frequency of the particle higher than 2 MHz only with a total laser input power of 60 μW. The demonstrated trap has its depth three times larger than the thermal energy at room temperature, and can be further equipped with readily available active stabilization schemes to ensure stable trapping of the particle in high vacuum environments. More remarkable is that the particle in our trap experiences factor of 43 less light intensity than conventional optical tweezers. It ensures that our trap exhibits significantly reduced optical absorption, a crucial requirement for quantum coherent experiments in high vacuum. Finally, by introducing multiple laser tones to each PCNC, we demonstrate the extraordinary versatility of our trapping system in creating complex potential landscapes with nanoscale resolutions. We also note that our PCNC-based trapping system is designed with realistic parameters, therefore, can be realized with available nanofabrication facilities. With all these unique features, our PCNC-based levitation system provides new directions in optical trapping and manipulation, particularly in the field of precision sensing and quantum experiments involving levitated particles.

Funding. Carl-Zeiss-Stiftung; Center for Integrated Quantum Science and Technology; Universität Stuttgart.

Acknowledgments. We thank Myungshik Kim and his group members, and Alessio Belenchia for fruitful discussions.

Disclosures. The authors declare no conflicts of interest.

Data Availability. The data that support this study are available upon reasonable request from the authors.

Supplemental document. See Supplement 1 for supporting content.

References

1. A. Ashkin, "Acceleration and trapping of particles by radiation pressure," Phys. Rev. Lett. **24**(4), 156–159 (1970).
2. W. D. Phillips, "Nobel lecture: Laser cooling and trapping of neutral atoms," Rev. Mod. Phys. **70**(3), 721–741 (1998).
3. A. Ashkin, J. M. Dziedzic, and T. Yamane, "Optical trapping and manipulation of single cells using infrared laser beams," Nature **330**(6150), 769–771 (1987).
4. D. E. Chang, C. A. Regal, S. B. Papp, D. J. Wilson, J. Ye, O. Painter, H. J. Kimble, and P. Zoller, "Cavity opto-mechanics using an optically levitated nanosphere," Proc. Natl. Acad. Sci. **107**(3), 1005–1010 (2010).
5. O. Romero-Isart, M. L. Juan, R. Quidant, and J. I. Cirac, "Toward quantum superposition of living organisms," New J. Phys. **12**(3), 033015 (2010).
6. U. Delić, M. Reisenbauer, K. Dare, D. Grass, V. Vuletić, N. Kiesel, and M. Aspelmeyer, "Cooling of a levitated nanoparticle to the motional quantum ground state," Science **367**(6480), 892–895 (2020).
7. L. Magrini, P. Rosenzweig, C. Bach, A. Deutschmann-Olek, S. G. Hofer, S. Hong, N. Kiesel, A. Kugi, and M. Aspelmeyer, "Real-time optimal quantum control of mechanical motion at room temperature," Nature **595**(7867), 373–377 (2021).
8. F. Tebbenjohanns, M. L. Mattana, M. Rossi, M. Frimmer, and L. Novotny, "Quantum control of a nanoparticle optically levitated in cryogenic free space," Nature **595**(7867), 378–382 (2021).
9. D. C. Moore, A. D. Rider, and G. Gratta, "Search for millicharged particles using optically levitated microspheres," Phys. Rev. Lett. **113**(25), 251801 (2014).
10. G. Ranjit, M. Cunningham, K. Casey, and A. A. Geraci, "Zeptonewton force sensing with nanospheres in an optical lattice," Phys. Rev. A **93**(5), 053801 (2016).
11. A. D. Rider, D. C. Moore, C. P. Blakemore, M. Louis, M. Lu, and G. Gratta, "Search for screened interactions associated with dark energy below the 100 μm length scale," Phys. Rev. Lett. **117**(10), 101101 (2016).
12. O. Romero-Isart, A. C. Pflanzer, F. Blaser, R. Kaltenbaek, N. Kiesel, M. Aspelmeyer, and J. I. Cirac, "Large quantum superpositions and interference of massive nanometer-sized objects," Phys. Rev. Lett. **107**(2), 020405 (2011).
13. Z.-q. Yin, T. Li, X. Zhang, and L. M. Duan, "Large quantum superpositions of a levitated nanodiamond through spin-optomechanical coupling," Phys. Rev. A **88**(3), 033614 (2013).

Optics EXPRESS

14. M. Scala, M. S. Kim, G. W. Morley, P. F. Barker, and S. Bose, "Matter-wave interferometry of a levitated thermal nano-oscillator induced and probed by a spin," Phys. Rev. Lett. **111**(18), 180403 (2013).
15. Y. Tsaturyan, A. Barg, E. S. Polzik, and A. Schliesser, "Ultracoherent nanomechanical resonators via soft clamping and dissipation dilution," Nat. Nanotechnol. **12**(8), 776–783 (2017).
16. A. H. Ghadimi, S. A. Fedorov, N. J. Engelsen, M. J. Bereyhi, R. Schilling, D. J. Wilson, and T. J. Kippenberg, "Elastic strain engineering for ultralow mechanical dissipation," Science **360**(6390), 764–768 (2018).
17. M. Aspelmeyer, T. J. Kippenberg, and F. Marquardt, "Cavity optomechanics," Rev. Mod. Phys. **86**(4), 1391–1452 (2014).
18. A. C. Frangeskou, A. T. M. A. Rahman, L. Gines, S. Mandal, O. A. Williams, P. F. Barker, and G. W. Morley, "Pure nanodiamonds for levitated optomechanics in vacuum," New J. Phys. **20**(4), 043016 (2018).
19. M. Barth and O. Benson, "Manipulation of dielectric particles using photonic crystal cavities," Appl. Phys. Lett. **89**(25), 253114 (2006).
20. M. L. Juan, R. Gordon, Y. Pang, F. Eftekhari, and R. Quidant, "Self-induced back-action optical trapping of dielectric nanoparticles," Nat. Phys. **5**(12), 915–919 (2009).
21. N. Descharmes, U. P. Dharanipathy, Z. Diao, M. Tonin, and R. Houdré, "Observation of backaction and self-induced trapping in a planar hollow photonic crystal cavity," Phys. Rev. Lett. **110**(12), 123601 (2013).
22. L. Neumeier, R. Quidant, and D. E. Chang, "Self-induced back-action optical trapping in nanophotonic systems," New J. Phys. **17**(12), 123008 (2015).
23. S. Mandal, X. Serey, and D. Erickson, "Nanomanipulation using silicon photonic crystal resonators," Nano Lett. **10**(1), 99–104 (2010).
24. S. Lin and K. B. Crozier, "Trapping-assisted sensing of particles and proteins using on-chip optical microcavities," ACS Nano **7**(2), 1725–1730 (2013).
25. L. Magrini, R. A. Norte, R. Riedinger, I. Marinković, D. Grass, U. Delić, S. Gröblacher, S. Hong, and M. Aspelmeyer, "Near-field coupling of a levitated nanoparticle to a photonic crystal cavity," Optica **5**(12), 1597 (2018).
26. P. B. Deotare, M. W. McCutcheon, I. W. Frank, M. Khan, and M. Lončar, "High quality factor photonic crystal nanobeam cavities," Appl. Phys. Lett. **94**(12), 121106 (2009).
27. M. Eichenfield, J. Chan, R. M. Camacho, K. J. Vahala, and O. Painter, "Optomechanical crystals," Nature **462**(7269), 78–82 (2009).
28. F. Liang, N. Clarke, P. Patel, M. Loncar, and Q. Quan, "Scalable photonic crystal chips for high sensitivity protein detection," Opt. Express **21**(26), 32306–32312 (2013).
29. J. Chan, A. H. Safavi-Naeini, J. T. Hill, S. Meenehan, and O. Painter, "Optimized optomechanical crystal cavity with acoustic radiation shield," Appl. Phys. Lett. **101**(8), 081115 (2012).
30. U. Delić, M. Reisenbauer, D. Grass, N. Kiesel, V. Vuletić, and M. Aspelmeyer, "Cavity cooling of a levitated nanosphere by coherent scattering," Phys. Rev. Lett. **122**(12), 123602 (2019).
31. T. Li, S. Kheifets, and M. G. Raizen, "Millikelvin cooling of an optically trapped microsphere in vacuum," Nat. Phys. **7**(7), 527–530 (2011).
32. J. Gieseler, B. Deutsch, R. Quidant, and L. Novotny, "Subkelvin parametric feedback cooling of a laser-trapped nanoparticle," Phys. Rev. Lett. **109**(10), 103603 (2012).
33. L. Rondin, J. Gieseler, F. Ricci, R. Quidant, C. Dellago, and L. Novotny, "Direct measurement of kramers turnover with a levitated nanoparticle," Nat. Nanotechnol. **12**(12), 1130–1133 (2017).